Helical CT image noise—analytical results

G. Wang and M. W. Vannier
Division of Radiology Research, Mallinckrodt Institute of Radiology, Washington University Medical School, St. Louis, Missouri 63110

(Received 5 March 1993; accepted for publication 8 July 1993)

Helical CT is an important recent development in x-ray CT. In helical CT, planar projection sets are synthesized from raw projection data via interpolation. Among various interpolation schemes, linear interpolation is usually preferred due to its efficiency and performance. In this paper, image noise variance is derived for typical helical CT linear interpolation techniques, including the full scan (FS), under-scan (US), full scan with interpolation (FI), half-scan (HS), half-scan with interpolation (HI) and half-scan with extrapolation (HE) methods. Image noise deviation ratios of helical CT to conventional 360° reconstruction (CR) are tabulated. These are consistent with previously reported simulation results. The theoretical results provide further understanding of helical CT noise performance. It is shown that helical CT image noise deviation is independent of transaxial position, proportional to the raw projection noise deviation, and not affected by the fan angle (approximately for the HE method). Also, helical CT image noise variance is proportional to the area under the square of the reconstruction filter.

Key words: computed tomography, helical scanning, spiral scanning, linear interpolation, noise

I. INTRODUCTION

Helical computed tomography (CT) is an important recent development in x-ray CT for rapid volumetric scanning.[1–4] In helical CT, source rotation and patient translation are performed simultaneously. Consequently, data acquisition time is reduced, retrospective reconstruction is allowed, and the longitudinal components of the reconstruction error are more evenly distributed. Another possible advantage of helical CT is a reduction in radiation hazard, since the maximum amount of radiation dose to individual cells is minimized. Due to these unique advantages, helical CT has been widely accepted clinically. However, helical CT has also some minor drawbacks. Depending on algorithms and imaging parameters (collimation, table increment, reconstruction interval, x-ray tube power, etc.), reconstructed images usually contain varying small amounts of longitudinal blurring and noise.

Helical CT image quality is essentially described in terms of spatial resolution and contrast resolution. The contrast resolution quantifies the ability to reveal small local attenuation changes in the human body, thus it is critically important for some clinical applications, such as lesion detection. The contrast resolution is directly affected by helical CT image noise.

Helical CT requires that planar projection sets be synthesized from raw projection data via interpolation. Among various interpolation techniques, linear interpolation is usually preferred due to its efficiency and performance. Typical linear interpolation techniques include full-scan (FS), under scan (US), full scan with interpolation (FI), half-scan (HS), half-scan with interpolation (HI) and half-scan with extrapolation (HE) methods.[3,5,6] In the FS method, raw projection data are collected at an angular range of 360° and undergo no modification before convolution and back-projection. Hence, the FS method is the simplest interpolation algorithm. The US and HS methods require the angular range to be 360° and 180° plus a fan angle, respectively. In both the US and the HS methods, raw projection data are underweighted near the beginning and end of a scan, compensated by overweighting projection data near the middle of the scan. In the FI method, a set of planar projection data in a 360° angular range is obtained via linearly interpolating neighboring raw projection data at the same orientation; hence the raw data involved span a 720° angular range. The HI method utilizes the redundancy of raw fan-beam data, interpolates neighboring raw data at opposite directions, and thus reduces the angular range from 720° required by the FI method to 360° plus two fan angles. The HE method eliminates the condition required by the HI method that the projection rays must be from different sides of a reconstruction plane. In the HE method, if the opposite rays are from the same side of the plane, extrapolation is performed to estimate the corresponding projection value; otherwise, still interpolation as in the HI method. Using the notations chosen by Kalender *et al.*, the FI and HI methods are equivalent to the 360LI and 180LI methods, respectively.[5,6] Among these linear interpolation methods, the US, HI, and HE methods are favored. Compared with others, these methods efficiently utilize raw data, reliably synthesize planar projections, and generally result in satisfactory reconstructed images.[3,5,6]

Previous studies on the relationship between the helical CT image noise and linear interpolation schemes were done either numerically or experimentally.[3,5–7] In this paper, image noise variance associated with typical linear

 0094-2405/93/20(6)/1635/6/$1.20

interpolation methods is derived. Image noise deviation ratios of helical CT to conventional 360° reconstruction (CR) are tabulated and discussed.

II. PROJECTION NOISE MODEL

Assume that the projection $P_\theta(t)$, as shown in Fig. 1, is corrupted by an additive white noise $v_\theta(t)$; then the measured projection $P_\theta^m(t)$ is expressed as

$$P_\theta^m(t)=P_\theta(t)+v_\theta(t), \tag{1}$$

and the correlation function

$$E[v_{\theta_1}(t_1)v_{\theta_2}(t_2)]=S_0\delta(\theta_1-\theta_2)\delta(t_1-t_2), \tag{2}$$

where S_0 is the noise spectrum density. Denote the Fourier transform of $v_\theta(t)$ as $N_\theta(w)$,

$$N_\theta(w)=\int_{-\infty}^{\infty} v_\theta(t)e^{-i2\pi wt}\,dt, \tag{3}$$

it follows that[8]

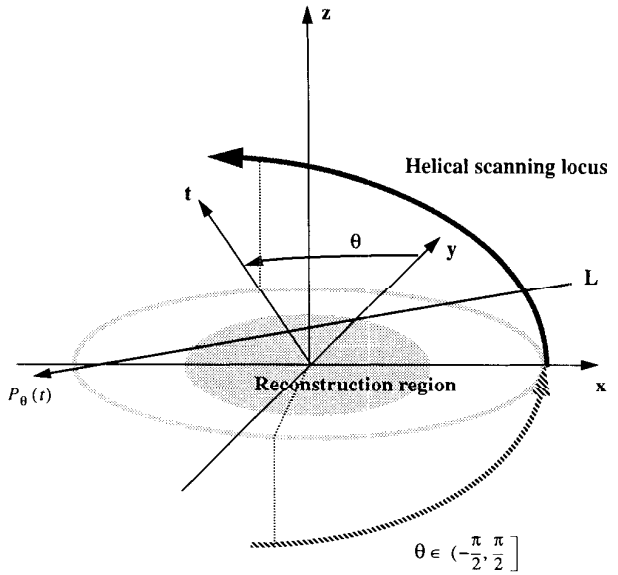

FIG. 1. The helical reconstruction coordinate system in the HI method. Projection $P_\theta(t)$ is the line integral along the ray L.

$$E[N_{\theta_1}(w_1)N_{\theta_2}^*(w_2)]=\int_{-\infty}^{\infty}\int_{-\infty}^{\infty} E[v_{\theta_1}(t_1)v_{\theta_2}(t_2)]e^{-i2\pi(w_1t_1-w_2t_2)}\,dt_1\,dt_2$$

$$=S_0\delta(\theta_1-\theta_2)\int_{-\infty}^{\infty}\int_{-\infty}^{\infty}\delta(t_1-t_2)e^{-i2\pi(w_1t_1-w_2t_2)}\,dt_1\,dt_2$$

$$=S_0\delta(\theta_1-\theta_2)\int_{-\infty}^{\infty}e^{-i2\pi(w_2-w_1)t}\,dt=S_0\delta(w_1-w_2)\delta(\theta_1-\theta_2). \tag{4}$$

III. IMAGE NOISE VARIANCE FORMULA

With a linear interpolation method, two independent white noise sources in the projection domain are linearly combined,

$$v_\theta(t,z)=a(\theta,t,z)v'_\theta(t)+b(\theta,t,z)v''_\theta(t), \tag{5}$$

where $a(\theta,t,z)$ and $b(\theta,t,z)$ are interpolation coefficients; functions of the rotation angle θ, the detector position t, and the slice longitudinal location z. It can readily be shown that the correlation function of $v_\theta(t,z)$ can be expressed in terms of the original noise spectrum density S_0 and the interpolation coefficient functions $a(\theta,t,z)$ and $b(\theta,t,z)$ as follows:

$$E[v_{\theta_1}(t_1,z)v_{\theta_2}(t_2,z)]=S_0[a(\theta_1,t_1,z)a(\theta_2,t_2,z)+b(\theta_1,t_1,z)b(\theta_2,t_2,z)]\delta(\theta_1-\theta_2)\delta(t_1-t_2)$$

$$=\sqrt{S_0[a^2(\theta_1,t_1,z)+b^2(\theta_1,t_1,z)]}\sqrt{S_0[a^2(\theta_2,t_2,z)+b^2(\theta_2,t_2,z)]}\delta(\theta_1-\theta_2)\delta(t_1-t_2)$$

$$=\sqrt{S_i(\theta_1,t_1,z)S_i(\theta_2,t_2,z)}\delta(\theta_1-\theta_2)\delta(t_1-t_2), \tag{6}$$

where

$$S_i(\theta,t,z)=S_0[a^2(\theta,t,z)+b^2(\theta,t,z)]. \tag{7}$$

Hence

$$E[N_{\theta_1}(w_1,z)N^*_{\theta_2}(w_2,z)]=E\left(\int_{-\infty}^{\infty} v_{\theta_1}(t_1,z)e^{-i2\pi w_1 t_1}\,dt_1\int_{-\infty}^{\infty} v_{\theta_2}(t_2,z)e^{+i2\pi w_2 t_2}\,dt_2\right)$$

$$=\int_{-\infty}^{\infty}\int_{-\infty}^{\infty} E[v_{\theta_1}(t_1,z)v_{\theta_2}(t_2,z)]e^{-i2\pi(w_1t_1-w_2t_2)}\,dt_1\,dt_2$$

$$=\int_{-\infty}^{\infty}\int_{-\infty}^{\infty}\sqrt{S_i(\theta_1,t_1,z)S_i(\theta_2,t_2,z)}\,\delta(\theta_1-\theta_2)\delta(t_1-t_2)e^{-i2\pi(w_1t_1-w_2t_2)}\,dt_1\,dt_2$$

$$=\delta(\theta_1-\theta_2)\int_{-\infty}^{\infty}\sqrt{S_i(\theta_1,t,z)S_i(\theta_2,t,z)}e^{-i2\pi t(w_1-w_2)}\,dt. \tag{8}$$

The image noise variance at the position z can be computed as follows:

$$\sigma^2_{\text{linear}}(z)=E[\,\hat{f}(x,y)-f(x,y)\,]^2$$

$$=E\left[\left(\frac{1}{k}\int_0^{k\pi}\int_{-\infty}^{\infty} N_\theta(w,z)|w|G(w)e^{i2\pi w(x\cos\theta+y\sin\theta)}dw\,d\theta\right)\right.$$

$$\left.\times\left(\frac{1}{k}\int_0^{k\pi}\int_{-\infty}^{\infty} N_\theta(w,z)|w|G(w)e^{i2\pi w(x\cos\theta+y\sin\theta)}dw\,d\theta\right)^*\right]$$

$$=\frac{1}{k^2}\int_0^{k\pi}\int_0^{k\pi}\int_{-\infty}^{\infty}\int_{-\infty}^{\infty}\left(\delta(\theta_1-\theta_2)\int_{-\infty}^{\infty}\sqrt{S_i(\theta_1,t,z)S_i(\theta_2,t,z)}e^{-i2\pi t(w_1-w_2)}\,dt\right)$$

$$\times|w_1w_2|G(w_1)G^*(w_2)e^{i2\pi[w_1(x\cos\theta_1+y\sin\theta_1)-w_2(x\cos\theta_2+y\sin\theta_2)]}d\theta_1\,d\theta_2\,dw_1\,dw_2$$

$$=\frac{1}{k^2}\int_0^{k\pi}\int_{-\infty}^{\infty}\int_{-\infty}^{\infty}\left(\int_{-\infty}^{\infty}S_i(\theta,t,z)e^{-i2\pi t(w_1-w_2)}\,dt\right)$$

$$\times|w_1w_2|G(w_1)G^*(w_2)e^{i2\pi(x\cos\theta+y\sin\theta)(w_1-w_2)}\,d\theta\,dw_1\,dw_2, \tag{9}$$

where $k=2$ for the CR, FS, US, and FI methods, $k=1$ for the HS, HI, and HE methods, and $G(w)$ is the smoothing filter used. Note that the parallel-beam reconstruction formula is used in computing the image noise variance. Actually, for a given set of projection data, the reconstructed image is the same whether using the parallel-beam reconstruction formula with the data organized in the parallel-beam projection format or using the fan-beam reconstruction formula with the data organized in the fan-beam projection format.

Averaging $\sigma^2_{\text{linear}}(z)$ with respect to z, we have

$$\sigma^2_{\text{linear}}=E_z[\sigma^2_{\text{linear}}(z)]=\frac{1}{k^2}\int_0^{k\pi}\int_{-\infty}^{\infty}\int_{-\infty}^{\infty}\left(\int_{-\infty}^{\infty}E_z[S_i(\theta,t,z)]e^{-i2\pi t(w_1-w_2)}\,dt\right)$$

$$\times|w_1w_2|G(w_1)G^*(w_2)e^{i2\pi(x\cos\theta+y\sin\theta)(w_1-w_2)}\,d\theta\,dw_1\,dw_2$$

$$=\frac{1}{k^2}\int_0^{k\pi}\int_{-\infty}^{\infty}\int_{-\infty}^{\infty}\left(\int_{-\infty}^{\infty}\bar{S}_i(t)e^{-i2\pi t(w_1-w_2)}\,dt\right)$$

$$\times|w_1w_2|G(w_1)G^*(w_2)e^{i2\pi(x\cos\theta+y\sin\theta)(w_1-w_2)}\,d\theta\,dw_1\,dw_2, \tag{10}$$

where we have used the fact that $E_z[S_i(\theta,t,z)] = E_\theta[S_i(\theta,t,z)] = E_{z,\theta}[S_i(\theta,t,z)]$, which depends upon neither z nor θ, and hence is denoted as $\bar{S}_i(t)$. Therefore, for a given linear interpolation method, if $\bar{S}_i(t)$ can be analytically determined, the image noise variance can be directly derived. In the CR method, $\bar{S}_i(t)=S_0$; hence we have

$$\sigma^2_{\mathrm{CR}}=S_0F, \tag{11}$$

where $F=(\pi/2)\int_{-\infty}^{\infty}|w|^2|G(w)|^2\,dw$. We will use σ_{CR} as a comparison standard for evaluating helical CT image noise deviations.

IV. IMAGE NOISE VARIANCES WITH FS, US, FI, HS, HI, AND HE METHODS

In the following derivation, we ignore the influence of the feathering algorithm, as the feathering distance is very small.[3] Let us start with the FS and HS methods. In both the FS and the HS methods, projection data are reconstructed without compensation for the table motion, that is, $\bar{S}_i(t)=S_0$; therefore we obtain immediately

$$\sigma^2_{\mathrm{FS}}=S_0F, \tag{12}$$

$$\sigma^2_{\mathrm{HS}}=2S_0F, \tag{13}$$

where the conventional 0–1 weighting function is assumed for the HS method. Note that σ^2_{HS} is the same as derived by Kak and Slaney.[8]

The US method is typically with the following weighting function:[3]

$$w(\beta,\gamma)=\begin{cases} 3x^2-2x^3, & x=\dfrac{\beta}{\beta_u}, \quad \beta\in[0,\beta_u]; \\ 1, & \beta\in(\beta_u,\pi-\beta_u-2\gamma]; \\ 2-(3x^2-2x^3), & x=\dfrac{|\beta-\pi+2\gamma|}{\beta_u}, \quad \beta\in(\pi-\beta_u-2\gamma,\pi+\beta_u-2\gamma]; \\ 1, & \beta\in(\pi+\beta_u-2\gamma,2\pi-\beta_u]; \\ 3x^2-2x^3, & x=\dfrac{2\pi-\beta}{\beta_u}, \quad \beta\in(2\pi-\beta_u,2\pi), \end{cases} \tag{14}$$

where β and γ denote the view and detector angles, and β_u is the under-scan angle. In this case, $\bar{S}_i(t)$ can be computed below:

$$\bar{S}_i(t)=\frac{2\pi-4\beta_u}{2\pi}S_0+\frac{2\beta_u}{2\pi}S_0\left(\int_0^1(3x^2-2x^3)^2\,dx+\int_0^1[2-(3x^2-2x^3)]^2\,dx\right)=\left(1+\frac{26}{35}\frac{\beta_u}{\pi}\right)S_0. \tag{15}$$

Hence

$$\sigma^2_{\mathrm{US}}=\left(1+\frac{26}{35}\frac{\beta_u}{\pi}\right)S_0F. \tag{16}$$

In the FI method, $\bar{S}_i(t)$ can be found by performing the integral

$$\bar{S}_i(t)=S_0\int_0^1[x^2+(1-x)^2]dx=\frac{2}{3}S_0. \tag{17}$$

Interestingly, $\bar{S}_i(t)$ with the HI method is also equal to $\frac{2}{3}S_0$. Figure 1 illustrates the helical reconstruction coordinate system used in the HI method. As shown in Fig. 2, for a given detector distance t, a 2π angular range of θ can be divided into two subintervals, $[-\phi,\pi+\phi)$ and $[\pi+\phi,2\pi-\phi)$, where $\phi=\tan^{-1}(t/\sqrt{D_{so}^2-t^2})$, D_{so} is the source-to-origin distance. In each subinterval, as θ increases from the minimum to the maximum, the position of the ray, along which the projection value is to be estimated, changes linearly from that of the upper helical ray to that of the lower one, while the distance between the upper and lower rays remains a constant. Then, we immediately obtain that $\bar{S}_i(t)=\frac{2}{3}S_0$, according to Eq. (17). Substituting $\bar{S}_i(t)=\frac{2}{3}S_0$ into Eq. (10) with $k=1$ and 2, we have

$$\sigma^2_{\mathrm{FI}}=\tfrac{2}{3}S_0F, \tag{18}$$

and

$$\sigma^2_{\mathrm{HI}}=\tfrac{4}{3}S_0F, \tag{19}$$

respectively.

In the case of the HE method, a closed form analytical solution is difficult to find. However, numerical computation shows that $\bar{S}_i(t)$ is very flat for typical helical CT parameters. When the ratio of the object radius over the

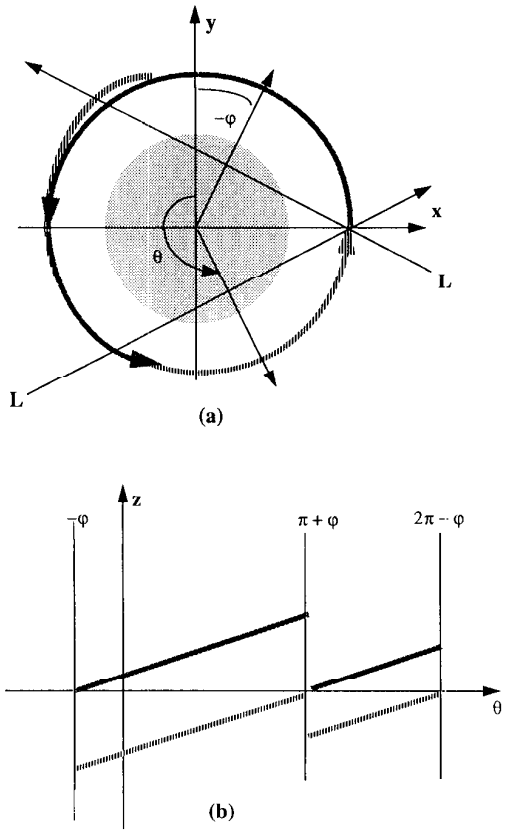

FIG. 2. In the HI method, the angularly averaged projection noise variance is independent of the detector position. (a) The whole angular range can be divided into two subintervals for a given detector position; (b) in each interval, the angularly averaged noise variance is two-thirds that in the original projection data.

source-to-origin distance was set to $\frac{1}{9}$ and $\frac{1}{2}$, the means of $\bar{S}_i(t)$ are 1.34 and 1.50, while their standard deviations are 0.08 and 0.003, respectively. Therefore,

$$\sigma^2_{\mathrm{HE}}=cS_0F, \tag{20}$$

where c is approximately between 1.34–1.50.

V. DISCUSSION AND CONCLUSION

The image noise variance associated with various interpolation methods are analytically derived. Image noise deviation ratios of helical CT to conventional 360° reconstruction (CR) are tabulated in Table I, which are consistent with previously reported simulation results.[3,5–7] Actually, using our formula (16) with the Crawford and King simulated data, the under-scan angle β_u can be estimated to be 44.0°, which is very close to the actual angle (45°) they used.[3] Our analytical results provide further understanding of the helical CT noise performance. It is observed that the helical CT image noise deviation is independent of the transaxial position, proportional to the raw projection noise deviation, and not affected by the fan angle (approximately for the HE method). Also, the helical CT image noise variance is proportional to the area under the square of the reconstruction filter $|wG(w)|$, which is expressed as $\int_{-\infty}^{\infty}|w|^2|G(w)|^2\,dw$. In order to reduce the noise variance in the reconstructed image, the smoothing filter $G(w)$ must be so chosen that the area under the square of $|wG(w)|$ is minimized before significant image details are blurred.

The analytical results obtained in this paper are practically very useful. For various interpolation methods and reconstruction filters, these noise variance formulas can be applied to estimate the noise performance approximately, which are more convenient than performing phantom measurements. In several helical CT applications including lesion detection, volume estimation, and image restoration, the theoretical characterization of the noise performance is important to model the imaging process. For example, when constrained least square restoration is performed longitudinally to enhance the resolution, the noise variance at any transverse position is needed in the constraint.[9] Our results justify the use of a constant noise variance in restoration.

Although the noise variance is typically used to describe the noise performance, the noise power spectrum is desirable in some cases. Also, a nonstationary Poisson noise model should be more accurate than the model used in this paper. Furthermore, the interpolation algorithms have different consequences with respect to not only noise but also contrast (some blur more than others). When a noise variance is smaller, the partial volume effect can be stronger as in the case of the FI method. To quantify the low contrast performance, a further analysis of these different interpolation methods should take both noise variation and contrast/detail degradation into consideration in the framework developed in this paper. All of these are worthy of further investigation.

TABLE I. Summary of image noise deviation ratios of helical CT to conventional 360° reconstruction. The algorithms involved are as follows: the conventional 360° reconstruction (CR), full scan (FS), under-scan (US), full scan with interpolation (FI), half-scan (HS), half-scan with interpolation (HI), and half-scan with extrapolation (HE). σ and σ' are used to represent, respectively, the theoretical deviations and the estimated ones using the Crawford and King simulated data (Ref. 3). In the computation of σ_{US}, β_u was set of $\pi/4$ (Ref. 3).

Method	CR	FS	US	FI	HS	HI	HE
$\frac{\sigma}{\sigma_{\mathrm{CR}}}$	1.00	1.00	$\sqrt{1+\frac{26}{35}\frac{\beta_u}{\pi}}\approx 1.09$	$\sqrt{\frac{2}{3}}\approx 0.817$	$\sqrt{2}\approx 1.41$	$\frac{2}{3}\sqrt{3}\approx 1.16$	$1.16\sim 1.23$
$\frac{\sigma'}{\sigma'_{\mathrm{CR}}}$	1.0	1.0	1.1	0.83	1.4	1.2	1.2

ACKNOWLEDGEMENTS

The authors would like to thank Dr. J. A. Brink for advice on the clinical significance of spiral CT, B. Brunsden, R. Knapp, and R. Walkup for their technical assistance in using software tools, and anonymous reviewers for their comments and suggestions on further research. Discussions with Dr. W. Kalender and Dr. C. Crawford on spiral/helical CT were helpful and are gratefully appreciated.

[1]Y. Bresler and C. J. Skrabacz, "Optimal interpolation in helical scan computed tomography," Proc. ICASSP **3**, 1472–1475 (1989).

[2]W. A. Kalender, W. Seissler, E. Klotz, and P. Vock, "Spiral volumetric CT with single-breath-hold technique, continuous transport, and continuous scanner rotation," Radiology **176**, 181–183 (1990).

[3]C. R. Crawford and K. F. King, "Computed tomography scanning with simultaneous patient translation," Med. Phys. **17**, 967–982 (1990).

[4]H. Rigaults, G. Marchal, A. L. Baert, and R. Hupke, "Initial experience with volume CT scanning," J. Comput. Assist. Tomog. **14**, 675–682 (1990).

[5]W. A. Kalender and A. Polacin, "Physical performance characteristics of spiral CT scanning," Med. Phys. **18**, 910–915 (1991).

[6]A. Polacin, W. A. Kalender, and G. Marchal, "Evaluation of section sensitivity profiles and image noise in spiral CT," Radiology **185**, 29–35 (1992).

[7]J. A. Brink, J. P. Heiken, D. M. Balfe, S. S. Sagel, J. DiCroce, and M. W. Vannier, "Spiral CT: Decreased spatial resolution *in vivo* due to broadening of section-sensitivity profile," Radiology **185**, 469–474 (1992).

[8]A. C. Kak and M. Slaney, *Principles of Computerized Tomographic Imaging* (IEEE, New York, 1987).

[9]A. K. Jain, *Fundamentals of Digital Image Processing* (Prentice-Hall, Engelwood Cliffs, NJ, 1989).